JACS
JOURNAL OF THE AMERICAN CHEMICAL SOCIETY
pubs.acs.org/JACS
Article

The Precise Synthesis of Ultradense Bottlebrush Polymers Unearths Unique Trends in Lyotropic Ordering

Timea Kolozsvary, Phillip Kohl,[‖] Tianyu Li,[‖] David Gillespie, Youli Li, and Benjamin R. McDonald*

Cite This: J. Am. Chem. Soc. 2025, 147, 889−897
Read Online

ABSTRACT: Biomacromolecular networks with multiscale fibrillar structures are characterized by exceptional mechanical properties, making them attractive architectures for synthetic materials. However, there is a dearth of synthetic polymeric building blocks capable of forming similarly structured networks. Bottlebrush polymers (BBPs) are anisotropic graft polymers with the potential to mimic and replace biomacromolecules such as tropocollagen for the fabrication of synthetic fibrillar networks; however, a longstanding limitation of BBPs has been the lack of rigidity necessary to access the lyotropic ordering that underpins the formation of collagenous networks. While the correlation between BBP rigidity and grafting density is well established, synthetic approaches to rigidify BBPs by increased grafting density are underdeveloped. To address this gap in synthetic capability, we report the synthesis of novel macroinitiators that provide well-defined BBPs with an unprecedentedly high grafting density. A suite of light scattering techniques are used to correlate macromolecular rigidity with grafting architecture and density and demonstrate for the first time that poly(norbornene) BBPs exhibit long-range lyotropic ordering as a result of their rodlike character. Specifically, the newly reported ultradensely grafted structures, preparable on multigram scale, form hexagonal arrays while conventional BBPs do not, despite showing long-range spatial correlations. These results implicate the central role of density and entanglement in the solution phase assembly of BBPs and provide new fundamental insight that is broadly relevant to the fabrication and performance of BBP-derived materials, spanning biomedical research to photonic materials and thermal management technologies. Furthermore, these newly reported liquid crystalline BBPs provide a structural template to explore the untapped potential of the bottom-up assembly of semiflexible networks and are ultimately intended to provide a modular route to hierarchically structured biomimetic materials.

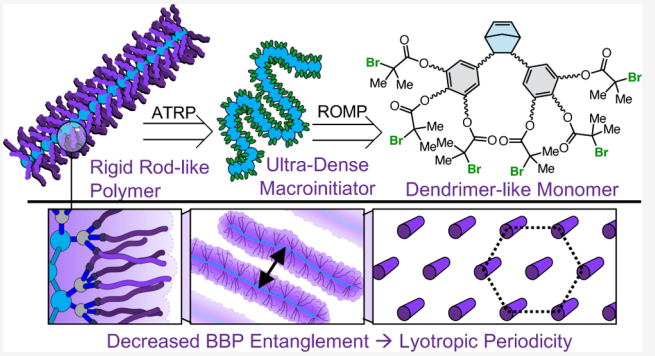

INTRODUCTION

Biomacromolecular networks have exceptional strength, toughness, and fracture resistance, as well as unique strain stiffening behavior features that are linked to their semiflexible fibrillar structure.[1−4] While networks that provide similar properties have been extensively pursued,[5−7] the ability to recapitulate the fundamental structure of biomacromolecular networks is still a challenge that if addressed could broadly impact areas spanning biomedical engineering and to electrochemical energy storage.[8−10] Structural mimicry of the constituent building blocks of biomacromolecular networks, such as tropocollagen and glycopolymers,[11−13] is an attractive approach to synthetic fibrillar networks.[8,9] To competently mimic the critical assembly processes that underlie fibrillar biomacromolecular network structure, candidate synthetic polymers should approximate the rodlike anisotropic shape of these building blocks and provide analogous solution phase behavior (Figure 1a).[14,15] Bottlebrush polymers (BBPs) are a class of graft polymer with the potential to match the shape and properties of biomacromolecules.[16−22] BBPs are characterized by a main chain with grafted side-chain polymers (SCPs), a topology that engenders unique physics and material properties. The dense packing of the SCP substituents along the main chain backbone of BBPs gives rise to reduced entanglement and supersoft elastomer behavior, as well as strain stiffening mechanics.[23−30] More generally, BBPs have potential applications as porous materials,[31−33] nanomaterial templates,[34] therapeutic and imaging delivery agents,[35,36] photonic materials,[37−39] and tissue engineering.[40,41] This expansive application space is made accessible by the rich array of well-developed methods for their precise preparation, such as reversible deactivation radical polymerization (RDRP) and ring-opening metathesis polymerization (ROMP); consequently, BBPs are an emerging platform for biomacromo-

Received: October 2, 2024
Revised: December 11, 2024
Accepted: December 12, 2024
Published: December 24, 2024

https://doi.org/10.1021/jacs.4c13759
J. Am. Chem. Soc. 2025, 147, 889−897

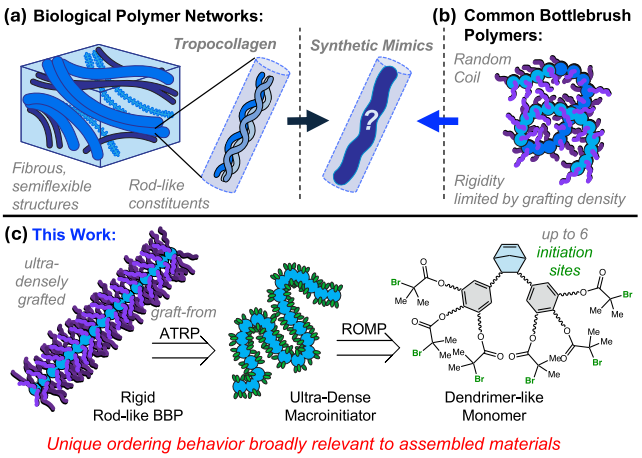

Figure 1. (a) Biomacromolecular networks are fibrous and semiflexible architectures composed of anisotropic constituents, such as tropocollagen, which demonstrates lyotropic liquid crystalline (LC) behavior that underpins its biological self-assembly. (b) Common bottlebrush polymers are characterized by random coil conformations in solution, preventing their use as LC biomacromolecule surrogates. (c) Ultradensely grafted BBP reported in this study shows unprecedented rodlike character and lyotropic ordering and are prepared via a precise bottom−up synthesis beginning with dendrimer-like monomers.

lecular surrogates.[17,23,27] Tropocollagen, a supramolecular complex of three linear peptide chains coaligned into a triple-helix structure, behaves as a colloidal liquid crystal, i.e., undergoes concentration-induced lyotropic ordering, due to its rodlike shape (300 nm) and considerable rigidity.[15] This liquid crystalline ordering underpins the structure and mechanics of the resulting fibrillar networks.[42,43]

BBP surrogates therefore should also be characterized by similar dimensions and rigidity to enable this important assembly behavior. Grafting density has been well demonstrated to significantly impact the melt[44,45] and solution phase conformation of BBPs;[18,46−48] however, only a few examples of BBPs exhibiting lyotropic ordering have been reported. These prior examples are limited to BBPs with polyvinyl backbones,[47,49] as the short repeat unit length (∼0.25 nm)[17] creates a dense environment. As a critical first step toward tropocollagen BBP surrogates, we sought a general, modular synthetic strategy. ROMP, characterized by high propagation rates and functional group tolerance, is an ideal synthetic method, as diverse compositions[11,50] can be arranged into exotic shapes[51] and ultralong structures, up to 7 μm in length.[26,52] However, the resulting polynorbornene backbones are more flexible than their polyvinyl analogues[45] and exhibit a more coiled solution conformation due to their longer backbone unit length (∼0.625 nm) (Figure 1b).[53] To address this fundamental limitation, we sought to prepare BBPs with as many as 6 chains per backbone unit (Figure 1c) and report herein an approach that provides multigram quantities of ultradense BBPs that show enhanced rodlike character and lyotropic ordering.

RESULTS AND DISCUSSION

Macroinitiator Synthesis. A *graft-from* approach, which involves polymerizing the SCP from initiation sites on the backbone polymer, was selected as it is well suited in the preparation of long and densely grafted BPPs.[26] However, initiation efficiency is a major concern with the *graft-from* approach, and the molecular design of the backbone macroinitiator (MI) is therefore critical.[54,55] To generate an ultradensely grafted BBP with multiple, uniform SCPs originating from each backbone (BB) repeat unit, macromonomers (MMs) were designed with a dendrimer-like molecular skeleton to mitigate steric restrictions associated with SCP initiation and growth.[56] The MM units consist of a singular norbornene ROMP moiety with α-dimethyl bromine atom-transfer radical polymerization (ATRP) initiation sites attached by phenoxy branch points. To compare the effects of grafting density on BBP solution behavior, two novel MI structures with 4 and 6 initiation points per backbone repeat unit were targeted and compared to the 2 initiation per unit structure, the most densely grafted conventional poly(norbornene) architecture.[45] The resulting BBPs are denoted by the following nomenclature: $_{GA}x\text{-}_{BB}y\text{-}_{SCP}z$, where GA refers to the grafting architecture of the MM (x = 2, 4, or 6 initiation

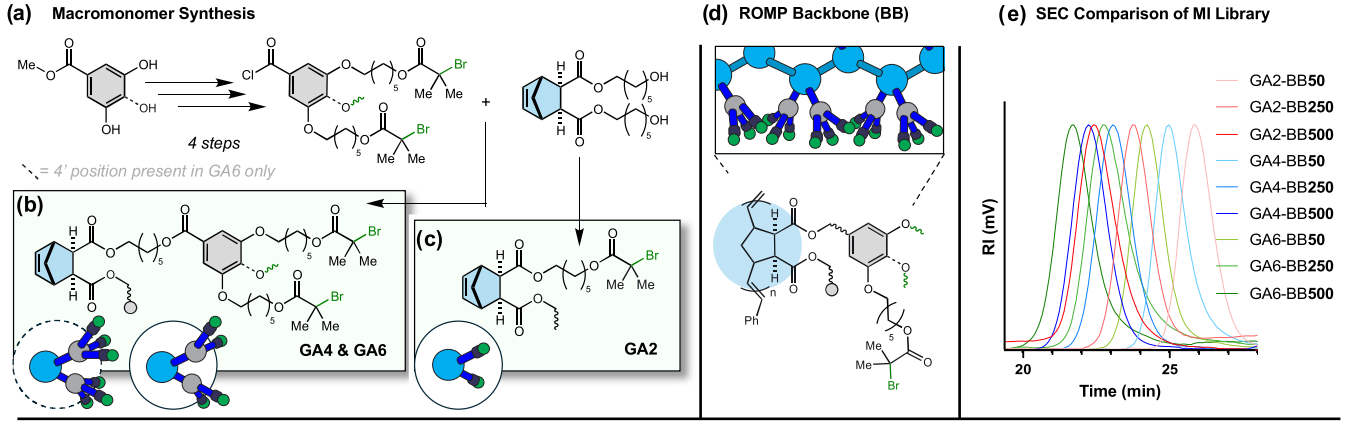

Figure 2. Macromonomer (MM) design and Macroinitiator (MI) Library. (a) Synthetic synopsis of MMs with the three grafting architectures surveyed (see the SI for experimental procedure and compounds SI-2, 11, and 12 for complete molecular design): (b) $_{GA}4$ and $_{GA}6$ MM design and schematic, where the dashed line at 4′ position indicates either a hydrogen atom or a third, identical initiation site, respectively. (c) $_{GA}2$ MM design and schematic. (d) Schematic of MM to MI polymerization via ROMP to form the backbone of the BBP. (e) Size exclusion chromatography (SEC) comparison of MI library shows single, low polydispersity peaks with minimal tailing and increasing molecular weight with backbone DP as high as 500 units, suggesting effective and efficient ROMP methodology (quantified in Table S1).

https://doi.org/10.1021/jacs.4c13759
J. Am. Chem. Soc. 2025, 147, 889−897

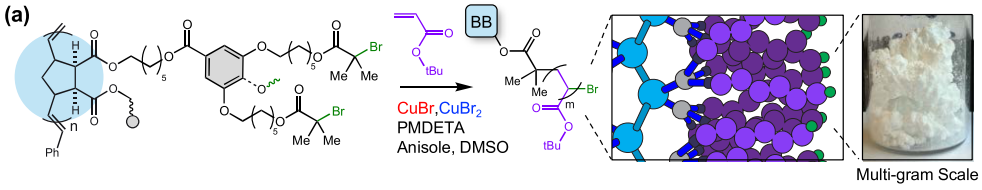

(b) **ATRP Optimization of *Grafting–From* Ultra-dense Macroinitiators**

ID	GA	◎ DP_{SCP}	tBA/Anisole	Cu_{total}	$CuBr_1/CuBr_2$	DP_{SCP}/h	DP_{SCP}	$Đ_{SCP}$	$\Delta Đ_{MI\rightarrow BBP}$
a	6	50	**100/900**	1	5:1	0.4	12*	*	<10
b	6	50	500/500	**0.5**	5:1	2.8	29*	*	<10
c	6	50	500/500	1	**20:1**	30.5	54	1.16	<10
d	6	**100**	500/500	1	9:1	39.0	160	1.55	>20
vi	6	100	1000/500	1	9:1	18.4	88	1.18	<25
iii	6	50	500/500	1	5:1	7.6	53	1.13	<5
ii	4	50	500/500	1	5:1	8.5	55	1.11	<5
i	2	50	500/500	1	5:1	10.5	53	1.10	<5

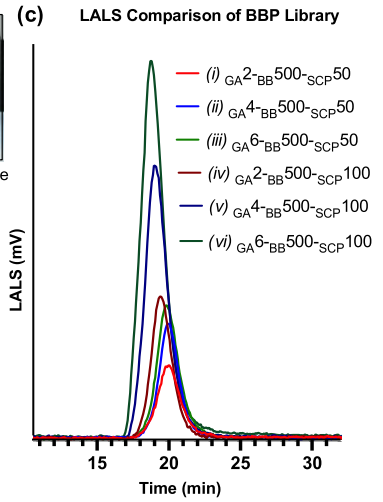

Figure 3. Atom-transfer radical polymerization (ATRP) design and analysis for BBP. (a) Synthetic synopsis for generating densely grafted poly(tBA) BBP using standard ATRP conditions and schematic and picture of isolated product BBP. (b) ATRP optimization for densely grafted BBP. * Indicates premature reaction termination observed via nonlinear degradative ATRP growth. The table displays BBP identity (ID), grafting architecture (GA), intended side-chain degree of polymerization as per design conditions (target DP_{SCP}), feed ratio of monomer to solvent (tBA/Anisole), equivalents of the total copper species with respect to initiation sites on the MI (Cu_{total}), ratio of activator to deactivator ($CuBr_1/CuBr_2$), rate of ATRP (DP_{SCP}/h), measured side-chain degree of polymerization (DP_{SCP}) and side-chain $Đ$ ($Đ_{SCP}$) as generated by SCP cleavage, and $\Delta Đ_{MI\rightarrow BBP}$ as percent increase in $Đ_{BBP}$ from $Đ_{MI}$ as measured by RI via SEC ($Đ_{BBP/MI}$), see Table S2. (c) LALS comparison of a library of BBP made with a constant DPBB of 500 and increasing GA and DP_{SCP} shows dramatically increasing molecular weights spanning from 10 to 40 million Dalton while maintaining single peaks with minimal tailing, suggesting no significant inter-BBP cross-linking. These samples are normalized by concentration (1 mg/mL). Note, samples *iv*, *v* corresponding to GA2 and GA4 DP_{SCP}100 were synthesized under identical conditions to sample *vi*.

sites per MM), BB refers to the backbone MI degree of polymerization ($y = DP_{MI}$), and SCP refers to the side-chain polymer degree of polymerization ($z = DP_{SCP}$). GA2MM has a total of two initiation sites (Figure 2c), while GA4 and GA6MM have two and three initiation sites branching from each arene loci, respectively (Figure 2b).

It was envisioned that each MM could share a common norbornene/hexanediol precursor (Figure 2a). GA2MM was prepared in two steps, with the reaction of hexanediol-norbornene with α-bromoisobutyryl chloride to attach a single unit of ATRP initiation site to the two arms of the MM. The synthesis of the GA4 and GA6MM is facilely completed in four additional steps from the common diol (Figure 2a) (see the Supporting Information (SI) for synthetic experimental details). The synthesis of these branched macromonomers is scalable with the final monomer generated on a 2 g scale and advanced intermediates on a decagram scale. However, careful attention to reagent selection and quality is required, particularly during the installation of the α-bromoisobutyryl moiety.[26] While, the *exo*-bis carboxylate structure utilized in these MMs is known to have a relatively moderate propagation rate in ROMP,[57,58] our early studies on the superior *exo*-bismethylene diol architecture proved synthetically challenging as the more constrained environment hindered the coupling of the branched units in the GA4 and GA6MM synthesis.

With our library of MMs in hand, attention was turned to their elaboration to MIs. A DP of 500 was chosen to approximately match the contour length of tropocollagen.[51] Initial screening of solvents identified ethyl acetate as the most effective solvent.[59] Despite their considerable mass and branched structure (MW GA4 = 1651.3 and GA6 = 2181.6 Da), complete polymerization of both GA4 and GA6 (DP_{500}) was observed within 60 min, with the extended linker structure likely obviating concerns of self-interruption.[60] Size exclusion chromatography (SEC) analysis of the resulting MI demonstrated a moderately low $Đ < 1.35$ of single peaks confirming expected MW (340−1,090 kDa) for all MMs (Figure 2e). Shorter MI prepared with DP_{50}, and DP_{250}, conversion was complete within 45 min or less and $Đ$ was <1.25. Thus, the MI library contains linear polymers with varying backbones of DP-50, 250, and 500, and with each backbone variety containing a set of three discrete grafting architectures: 2, 4, or 6 ATRP initiation sites at each repeat unit.

Bottlebrush Synthesis. To successfully prepare the targeted ultradensely grafted BBPs, SCPs must be polymerized uniformly from each ATRP initiation site. *Grafting-from* via RDRP presents two key challenges toward this, uniformity of initiation and radical−radical coupling reactions between the growing chain ends, which may lead to intra-BBP SCP termination or inter-BBP dimerization (Figure S2a).[54] Considering that our MIs contain 1000, 2000, and 3000 initiation sites, respectively, this posed a substantial challenge. Given this ultradense display of initiation sites, we anticipated that even a small number of cross-coupling events between these megadalton molecules would quickly lead to nanogels that exceed solubility thresholds.[61,62] These considerations indicated that these reactions would require substantially dilute conditions with respect to the developing BBPs, with each initiation site being rapidly activated and deactivated. Gratifyingly, the array of well-developed ATRP conditions provided ample options to carefully tune these reaction parameters.[63] Due to the specific desire to tune the activator:deactivator ratio as well as overall copper concentration, conventional ATRP methods were selected and *N*,*N*,*N*′,*N*″,*N*″-pentamethyldiethylenetriamine (PMDETA) was chosen as the ligand for its high rate of deactivation.[63] While an impressive array of photo-ATRP methods continue to be developed,[64−67] they have shown modest initiation efficiencies in *grafting-from* regimes

https://doi.org/10.1021/jacs.4c13759
J. Am. Chem. Soc. 2025, 147, 889−897

(ca. 70−80%).[68] The low copper loading likely results in slow chain deactivation, with rapid SCP extension hindering the initiation of other SCPs, underscoring the need for careful control of RDRP parameters in *grafting-from*. For the preparation of our BBPs, ATRP was conducted in anisole, using high equivalents of monomer *tert*-butyl acrylate (Figure 3a). ATRP rate and behavior have been assessed with respect to the ratio of total copper catalyst to initiation sites, the ratio of copper catalyst activator to deactivator, reaction concentration, and the ratio of initiation sites to available monomer, or feed ratio (Figure 3b).

The sum of activating and deactivating species was selected to be equimolar to the total number of initiation sites to provide an ideal initiation efficiency. Lower catalyst loading reduced the rate of chain growth as expected, and self-termination events were observed as the ATRP rate decayed over time and was unable to reach target conversion (Figure 3b, entry b). The most success was found with a 5:1 activator:deactivator ratio, which is a relatively high ratio of deactivator compared to traditional standard ATRP techniques.[26,54,69−71] With higher loading of activator, competent BPP production is retained, but batch-to-batch consistency is difficult, as quenching the ATRP at the targeted DP is challenging given the accelerated rate of SCP growth (Figure 3b, entry c).

The identity as well as concentration of the solvent impact not only the ATRP rate but also the persisting solvation of the increasingly densely grafted BBP. Excess monomer, *tert*-butyl acrylate (tBA) ensures BBP solubility and is favorable for polymerization fidelity. Approximately 10% conversion of monomer to BBP-SCP was targeted for all grafting architectures, and for all SCP-lengths (Figure 3b, entries i−iii, vi), when the equivalents of monomer are reduced, increased termination slows the rate of ATRP and the reaction stalls (Figure 3b, entry a). Feed ratio and BBP concentration are also predominant design considerations. The considerable size and rigidity of the BBPs cause sample viscosity to increase rapidly, facilitating BBP coupling and rapid gelation. This is readily visible in the attempted synthesis of DP_{100} samples, whereby attempting to extend the reaction to 20% conversion (rather than 10%) within the reaction conditions designed for target DP_{50} BBP, results in polydisperse and cross-linked BBP (Figure 3b, entry d). The stoichiometric excess of monomer is helpful to drive the reaction toward the polymerization, and flexibility in the ratios of activator and deactivator allows for practical adjustment of k_{ATRP} around modification parameters. Under the optimized conditions, monomer conversion is approximately linear (Figure S5) and resulting materials elute as a single peak on SEC, free from significant cross-linking (Figure 3c), and are conveniently collected as white powders (Figure 3a) via precipitation from a solution of 20% water in methanol (Figure S2b) and up to 5 g scale.

Structure Validation. For each BBP prepared under the optimized conditions, the SEC-MALS elutogram displays a singular peak that reflects the approximate $Đ$ of the respective MI and demonstrates orders of magnitude of growth in MW as expected per SCP length and grafting density, suggesting that dimerization or cross-linkage between MI is negligible (Figure 3c and Table S2). However, characterization of the BBP is not sufficient by SEC alone, as SEC has been shown to be relatively insensitive to BBP chain dispersity.[72] Sensitivity to variations in grafting efficiency and density, such as the dispersity of the individual side chains, is of critical importance for verifying these ultradense designs. Cleavage of brushes via bulk Fisher transesterification with an alcohol and analysis of the resulting linear polymers via SEC has been demonstrated to provide exquisite insight into molecular weight and dispersity of the brushes (Figure 4a).[54] In initial studies, the transesterification reaction was run for ∼100 h as previously reported and showed a bimodal distribution, indicating an alarming potential for intramolecular SCP cross-linking. To further investigate this observed cleavage phenomena, a star polymer model of a single BBP repeat unit was prepared for the GA4 and GA6 systems and subjected to the same cleavage reaction, but with an extension of the digestion time to ∼215 h, monitoring reaction progress with SEC. A stable SCP MW is reached, and BBP and star polymer SCP and cleavage patterns are observed to match one another (Figure 4b,c), which suggests that despite the dense architecture, the BBP design is a permeable and fully solvated construct, and that the long time-scale required for cleavage is a product of the chemistry of the ester species in the GA4 and GA6 macromonomers themselves.

Importantly, $_{GA}2\text{-}_{SCP}50$, $_{GA}4\text{-}_{SCP}50$, and $_{GA}6\text{-}_{SCP}50$ all converge to the same molecular weight and show similar elutograms (Figure 4d,e). That is, all BBP decomposition patterns show a consistent low molecular weight peak, comparable between each GA with a constant SCP_{DP} which supports the notion of uniformly grafted species (Figure 4f, entry E_G). The GA6 BBP shows slightly higher SCP dispersity than the GA2 and GA4 systems, owing to the increased likelihood of termination events during ATRP due to the density of the six SCPs (Figure 4f, entry$Đ_{SCP}$). Nevertheless, as the ultradensely grafted BBPs show comparable SCP size and dispersity to the conventional structure, this novel monomer design is validated as a robust approach to ultradensely grafted BBPs (Figure 4f).

As these macromolecules are expected to span approximately 300 nm at their longest dimension (based on a backbone DP_{BB} ∼500 and repeat unit length of ∼0.625 nm), atomic force microscopy (AFM) offers a qualitative approach to verifying the BBP as an independent macromolecular construct. BBP samples were converted from poly(t-Butyl acrylate) SCP to poly(acrylic acid) in order to affix BBPs to freshly cleaved mica and then were viewed in scanning mode using AFM. Sample dimensions and uniformity corresponding to ROMP and ATRP parameters are highlighted (Figure S9). While precise and quantitative comparisons of these surface-adsorbed BBPs can be made,[73] a direct analysis of the solution phase behavior of these compounds is of greatest interest as lyotropic ordering behavior is predicated by their solution phase properties, namely, aspect ratio, rigidity, and solvation.[74]

Characterization of Solution Structure and Lyotropic Ordering. Multiangle light scattering (MALS) in conjunction with SEC was employed to first characterize the solution phase properties of our library of BBPs. In addition to the determination of their absolute molecular weight, the relative differences in scattering intensity at multiple observation angles are also indicative of macromolecular shape in solution.[75] By fitting the observed BBP scattering profiles to the theoretical profiles of rods, random coils, and spheres, a rodlike character can be assigned, as a fraction of the observed population (P_{rod}) (see Supporting Information Methods for more details, see Sing et al. for a comprehensive overview on the modeling of bottlebrush structure and characterization of solution conformation[22]).

https://doi.org/10.1021/jacs.4c13759
J. Am. Chem. Soc. 2025, 147, 889−897

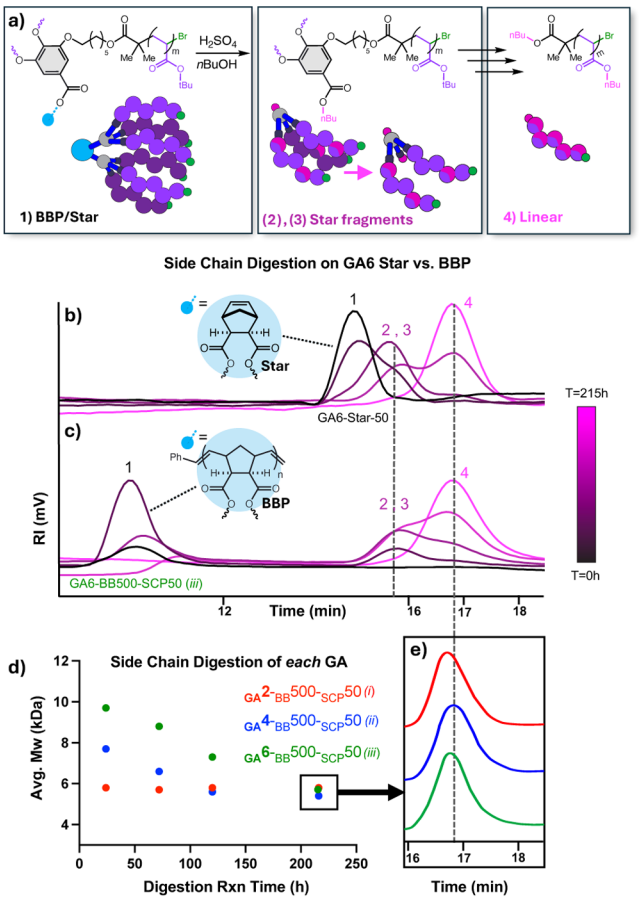

f) BBP Individual Characterization

ID	GA	DP_{SCP}	E_G	$Đ_{SCP}$	$Đ_{BBP}$
i	2		106	1.10	1.30
ii	4	50	110	1.11	1.33
iii	6		106	1.13	1.46
iv	2		115	1.15	1.33
v	4	100	107	1.20	1.48
vi	6		105	1.18	1.72

Figure 4. Analysis of the SCP cleavage from BBP. (a) Schematic of segmented decomposition via *n*-butyl transesterification in $_{GA}6$ polymer architecture resulting in linear SCP. (b) SEC analysis depicts elutograms of star polymer $_{GA}6$-$_{BB}0$-$_{SCP}50$ and (c) BBP polymer $_{GA}6$-$_{BB}500$-$_{SCP}50$ at SCP cleavage time points from 0 to 215 h (overlaid), demonstrating a parallel digestion pattern, indicating both BBP permeability as well as similar grafting efficiency regardless of polymerization from either MM or MI within the most dense GA framework. (d) SCP cleavage comparison of varying GA's reveals: (e) final linear polymers with matching elution times, indicating similar grafting efficiencies regardless of GA, despite the initial difference in decomposition profile (d). (f) SCP cleavage allows for characterization of individual BBPs as portrayed by the grafting efficiency (E_G), and $Đ$ of the side chains ($Đ_{SCP}$) as well as BBP ($Đ_{BBP}$). E_G values lower than 100% imply cleaved SCP are larger than expected based on monomer conversion, meaning some initiation sites may not have produced "full-length" SCP. E_G values greater than 100% imply that cleaved SCP are smaller than suggested by monomer conversion and may be artifacts of monomer evaporation and error within NMR conversion.

As such, the relative effects of both SCP_{DP} and GA, which both impact the overall rigidity, may be systematically compared (Figure 5a,b). It is important to note that a difference in BBP scaling rigidity is to be expected between

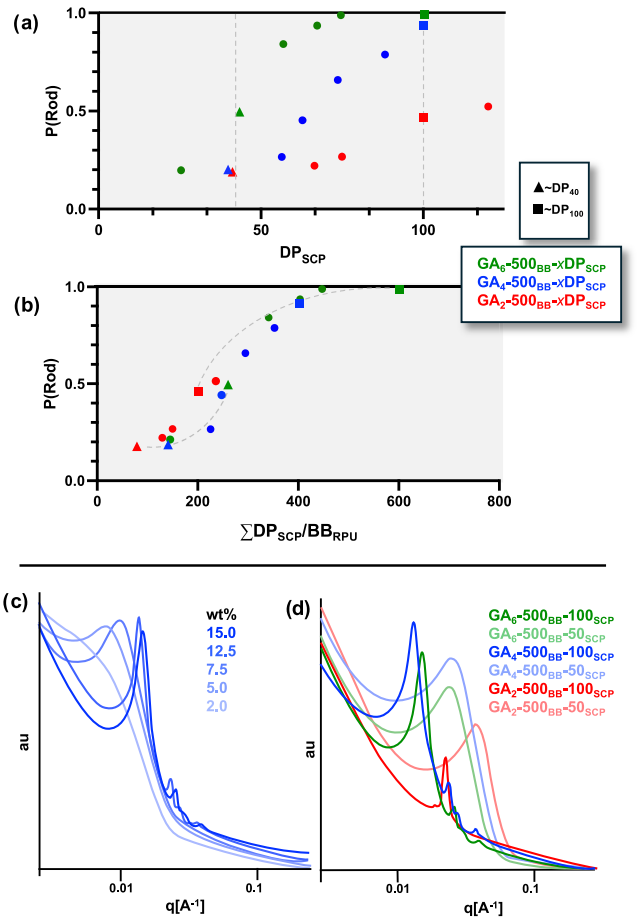

Figure 5. BBP rigidity and periodicity via MALS and SAXS respectively. Percent rodlike (P_{Rod}) behavior as a function of GA and (a) total DP_{SCP} per each initiation site; (b) total DP_{SCP} units per backbone repeat unit, which demonstrates the scaling relationship as a function of GA (dashed lines added for trend visualization purposes). (c) SAXS signal of $_{GA}4$-$_{BB}500$-$_{SCP}100$ at various concentrations. (d) $_{GA}(2,4,6)$-$_{BB}500$-$_{SCP}(50,100)$ samples at 15% wt. BBP intercorrelation peak is observable for all samples at and above 5% wt. Bragg peaks corresponding to a 2D hexagonal lattice are seen for $_{GA}(2,4,6)$-$_{BB}500$-$_{SCP}100$ samples above 7.5% wt.

GA2 compared to GA4 and GA6 due to the variability in the distance of the ATRP initiation site from the backbone, with a larger displacement resulting from the addition of arene branching loci in the GA4 and GA6 system.[53] When SCP-DP is held constant, the impact of the grafting architecture can be evaluated (Figure 5a). For example, in GA2, 4, and 6 BBPs, where $_{BB}500$-$_{SCP}50$, P_{rod} is calculated to be ~0.15, 0.25, and 0.60 respectively, showing that each increase in BBP density (ca. 1000, 2000, 3000 brushes per BBP, respectively) effectively doubles the population of rodlike object in solution. Thus, the denser grafting architecture allows for BBP with higher P_{rod} at lower SCP-DP, which is a critical distinction in the pursuit of high aspect ratio BBPs, as our studies indicate that ~$_{SCP}100$ is around the maximum SCP-DP that can be prepared on a multigram scale. It is important to note that SCP substituent identity will shift the (P_{rod})− SCP-DP scaling. Future studies will examine these relationships with

https://doi.org/10.1021/jacs.4c13759
J. Am. Chem. Soc. 2025, 147, 889−897

compositions that mimic those of biomacromolecules, namely, charge and attractive intermolecular interactions.

Additionally relevant to rodlike biomacromolecular mimicry are disorder−order transitions that occur in critical concentrations dictated by their aspect ratio, stiffness, and solvation.[15,74] To characterize how the observed rodlike character of the synthesized BBPs would translate to lyotropic ordering, solutions varying in concentration (2−15 wt %) of six BBP $_{GA}$(2,4,6)-$_{BB}$500-$_{SCP}$(50,100) were prepared and subjected to analysis by small-angle X-ray scattering (SAXS).

In the dilute regime (∼2 wt %), SAXS data from all BBPs displayed a Guinier type of scattering profile (Figure S11), which was modeled by a characteristic R_g (radius of gyration). Due to the inherently high aspect ratio (backbone length/side-chain length) of the molecule, it is reasonable to assume that the observed R_g values are determined primarily by the cylindrical diameter of the rodlike BBP (Table S5). As expected, the rod diameter scales almost proportionally with the side-chain length (the diameter values of 100-unit side chain are ∼2 times those of 50-unit side chain). There is a smaller but observable increase in the rod diameter with increasing grafting density. This behavior is consistent with the expectation that as the grafting density increases, the lateral degree of freedom of the side chains is reduced, leading to more extended chains and larger diameter.

The emergence of a broad correlation peak was observed for each BBP at 5 wt % (Figure S11). This correlation peak defines the center-to-center distance, between neighboring BBPs and was observed to decrease with increasing BPP concentrations (Figure S14a). At 12.5 wt % and above, $_{GA}$(2,4,6)-$_{BB}$500-$_{SCP}$100 all showed signs of lyotropic ordering, indicated by the sharpening of the correlation peak and appearance of higher-order peaks (in some cases) (Figure 5d). However, the $_{GA}$(2,4,6)-$_{BB}$500-$_{SCP}$50 BBP solutions remained disordered, showing only broad correlation peaks due to their much lower rigidity compared to the $_{SCP}$100 samples. Interestingly, the ultradense $_{GA}$4 and $_{GA}$6-$_{BB}$500-$_{SCP}$100 displayed higher-order Bragg peaks indicative of hexagonal ordering, whereas $_{GA}$2-$_{BB}$500-$_{SCP}$100 did not (Figure 5d), despite having a much sharper first-order Bragg peak. Notably, domain size is inversely proportional to the width of the characteristic Bragg peak and thus implies that the $_{GA}$2-$_{BB}$500-$_{SCP}$100 has the longest-range order of all samples. Long-range order without the existence of higher-order Bragg peaks is a result of a pseudosinusoidal electron density function—which can occur with a high degree of interpenetration of SCPs between neighboring BBPs. As such, a lower grafting density could be more conducive to side-chain interpenetration because of the larger separation between the chains along the rod (Figure 6a,b). Indeed, a comparison of the BBP center-to-center distance at 15 wt % (23.8 nm at) to the hard cylindrical diameter (41.1 nm) for $_{GA}$2-$_{BB}$500-$_{SCP}$100 confirms a high degree of SCP interdigitation (Figure S14a). Brush intertwinement was progressively less with increased grafting density and decreased SCP length with $_{GA}$6-$_{BB}$500-$_{SCP}$50s interaxial distance (21.5 nm) very close to the hard cylindrical diameter (22.8 nm) (Figure S14b).

These systematic studies suggest that in addition to changes in rigidity, the molecular architecture of the denser systems may also lend itself to periodic solution conformation, whereby less densely grafted systems are more capable of forming intermolecular brush intertwinement at increasing concentrations, compared to more densely grafted counterparts, serving as a kinetic barrier to the formation of energetically favored ordered arrays. This raises intriguing questions on the differences in SCP conformation and dynamics as a function of grafting density, with these data suggesting systems composed of a few, long brushes and systems with multiple, shorter SCPs behave substantially differently. This could have profound impacts on intra- and inter-BBP interactions, particularly in systems containing noncovalent interactions, which will in turn have substantial impacts on the structure and mechanics of their resulting networks.[14,28] This work as well as subsequent studies are anticipated to be of broad relevance as the rigidity and density of bottlebrushes are important to their function in many contexts; their function as nanoparticles with biomedical relevance, *in vivo* lifetime/pharmacokinetics,[35] contrast agents,[36] drug delivery;[76] as nanomaterial templates;[34] and as assembled photonic[37−39] and porous materials.[33]

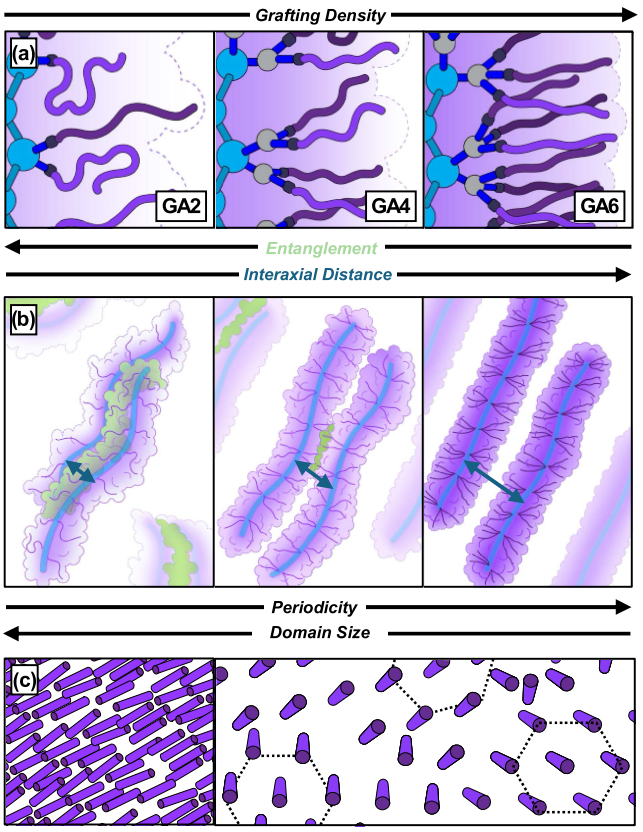

Figure 6. Schematic of the GA impact across length scales. (a) Increasing density from GA_2 → GA_6 increases the steric bulk around BBP backbone, which correlates with (b) interaxial spacing between neighboring BBP suggested to be a result of a diminished inter-BBP entanglement via steric accessibility. (c) Increased domain sizes are observed at lower grafting densities, but higher-order hexagonal periodicity is observed with increased grafting density, suggesting that entanglements play a role in the ability to form higher-order arrangements.

CONCLUSIONS

In summary, the strategic application of well-developed polymer chemistries on unique molecular skeletons has granted access to BBPs with unprecedentedly high grafting density on a multigram scale. Chemical degradation studies in conjunction with SEC-MALS analysis were used to confirm

https://doi.org/10.1021/jacs.4c13759
J. Am. Chem. Soc. 2025, 147, 889−897

their structure as well as systematically elucidate the rigidity contributions of the grafting architecture relative to the side-chain degree of polymerization. SAXS analysis further demonstrated such BBPs are capable of long-range hexagonal ordering as consistent with a high P_{rod} value and further showed intriguing differences in lyotropic organization as a function of grafting density that will have substantial impacts on network scale properties and impinges on a variety of important material driven technologies. Finally, these novel lyotropic LC BBPs offer multiple axes of modularity in their dimensions, rigidity, and interbrush entanglement, granting novel access to the development of modular biomacromolecular surrogates capable of self-assembly. We look forward to merging these macromolecular design parameters with the chemical processes of semiflexible fibrillar network assembly and reporting in due time on the formation of hierarchically ordered biomimetic materials.

■ ASSOCIATED CONTENT

Supporting Information

The Supporting Information is available free of charge at https://pubs.acs.org/doi/10.1021/jacs.4c13759.

General experimental procedures and detailed synthetic procedures and characterization and additional data (PDF)

■ AUTHOR INFORMATION

Corresponding Author

Benjamin R. McDonald − *Department of Chemistry at Brown University, Providence, Rhode Island 02912, United States;* orcid.org/0000-0002-2408-2448; Email: mcdonabe@brown.edu

Authors

Timea Kolozsvary − *Department of Chemistry at Brown University, Providence, Rhode Island 02912, United States;* orcid.org/0000-0002-0960-9985

Phillip Kohl − *Materials Research Laboratory at UC Santa Barbara, Santa Barbara, California 93106, United States*

Tianyu Li − *TOSOH Bioscience Inc., King of Prussia, Pennsylvania 19406, United States;* orcid.org/0000-0003-2324-6452

David Gillespie − *TOSOH Bioscience Inc., King of Prussia, Pennsylvania 19406, United States*

Youli Li − *Materials Research Laboratory at UC Santa Barbara, Santa Barbara, California 93106, United States;* orcid.org/0000-0001-5117-3874

Complete contact information is available at: https://pubs.acs.org/10.1021/jacs.4c13759

Author Contributions

‖P.K. and T.L. contributed equally to this work. The manuscript was written through contributions of all authors. All authors have given approval to the final version of the manuscript.

Funding

This work was funded by Rhode Island IDeA Network of Biomedical Research Excellence (NIH Award No: 5P20GM103430−22, Sub-Award No: 0009701/07152022A) and start-up funds from Brown University. The research reported here made use of shared facilities of the NSF BioPACIFIC Materials Innovation Platform of the National Science Foundation under Award No. DMR-1933487.

Notes

The authors declare no competing financial interest.

■ ACKNOWLEDGMENTS

We thank Prof. Eric Darling for the use of their atomic force microscope.

■ ABBREVIATIONS

BBP, bottlebrush polymer; MM, macromonomer; MI, macroinitiator; BB, backbone; GA, grafting architecture; GA2, grafting architecture 2; GA4, grafting architecture 4; GA6, grafting architecture 6; SCP, side-chain polymer; ROMP, ring-opening metathesis polymerization; RDRP, reversible deactivation radical polymerization; ATRP, atom-transfer radical polymerization; t(BA), t-butyl acrylate; DP, degree of polymerization; $Đ$, dispersity; SEC, size exclusion chromatography; MALS, multiangle light scattering; LALS, low-angle light scattering; RALS, right-angle light scattering; HALS, high-angle light scattering; RI, refractive index; R_G, radius of gyration; mV, millivolts; P_{rod}, percent rodlike nature; SAXS, small-angle X-ray scattering; au, absorbance units; nm, nanometers; MW, molecular weight; PMDETA, *N*,*N*,*N*′,*N*″,*N*″-pentamethyldiethylenetriamine; Circle ring operator DP, targeted degree of polymerization; $Đ_{SCP}$, side-chain polymer polydispersity index; $Đ_{BBP}$, bottlebrush polymer polydispersity index; BB_{RPU}, bottlebrush polymer repeat unit; E_G, grafting efficiency

■ REFERENCES

(1) Zhao, X. H.; Chen, X. Y.; Yuk, H.; Lin, S. T.; Liu, X. Y.; Parada, G. Soft Materials by Design: Unconventional Polymer Networks Give Extreme Properties. *Chem. Rev.* **2021**, *121*, 4309−4372.

(2) Yang, W.; Sherman, V. R.; Gludovatz, B.; Schaible, E.; Stewart, P.; Ritchie, R. O.; Meyers, M. A. On the tear resistance of skin. *Nat. Commun.* **2015**, *6*, No. 6649.

(3) Brown, A. E. X.; Litvinov, R. I.; Discher, D. E.; Purohit, P. K.; Weisel, J. W. Multiscale Mechanics of Fibrin Polymer: Gel Stretching with Protein Unfolding and Loss of Water. *Science* **2009**, *325*, 741−744.

(4) Jansen, K. A.; Licup, A. J.; Sharma, A.; Rens, R.; MacKintosh, F. C.; Koenderink, G. H. The Role of Network Architecture in Collagen Mechanics. *Biophys. J.* **2018**, *114*, 2665−2678.

(5) Jaspers, M.; Dennison, M.; Mabesoone, M. F. J.; MacKintosh, F. C.; Rowan, A. E.; Kouwer, P. H. J. Ultra-responsive soft matter from strain-stiffening hydrogels. *Nat. Commun.* **2014**, *5*, No. 5808.

(6) Vatankhah-Varnosfaderani, M.; Daniel, W. F. M.; Everhart, M. H.; Pandya, A. A.; Liang, H.; Matyjaszewski, K.; Dobrynin, A. V.; Sheiko, S. S. Mimicking biological stress−strain behaviour with synthetic elastomers. *Nature* **2017**, *549*, 497−501.

(7) Li, X.; Gong, J. P. Design principles for strong and tough hydrogels. *Nat. Rev. Mater.* **2024**, *9*, 380−398.

(8) Prince, E.; Kumacheva, E. Design and applications of man-made biomimetic fibrillar hydrogels. *Nat. Rev. Mater.* **2019**, *4*, 99−115.

(9) Khuu, N.; Kheiri, S.; Kumacheva, E. Structurally anisotropic hydrogels for tissue engineering. *Trends Chem.* **2021**, *3*, 1002−1026.

(10) Soliman, B. G.; Nguyen, A. K.; Gooding, J. J.; Kilian, K. A. Advancing Synthetic Hydrogels through Nature-Inspired Materials Chemistry. *Adv. Mater.* **2024**, No. e2404235.

(11) Kruger, A. G.; Brucks, S. D.; Yan, T.; Cárcarmo-Oyarce, G.; Wei, Y.; Wen, D. H.; Carvalho, D. R.; Hore, M. J. A.; Ribbeck, K.; Schrock, R. R.; Kiessling, L. L. Stereochemical Control Yields Mucin Mimetic Polymers. *ACS Cent. Sci.* **2021**, *7*, 624−630.

(12) Banquy, X.; Burdyńska, J.; Lee, D. W.; Matyjaszewski, K.; Israelachvili, J. Bioinspired Bottle-Brush Polymer Exhibits Low Friction and Amontons-like Behavior. *J. Am. Chem. Soc.* **2014**, *136*, 6199−6202.
(13) Adibnia, V.; Olszewski, M.; De Crescenzo, G.; Matyjaszewski, K.; Banquy, X. Superlubricity of Zwitterionic Bottlebrush Polymers in the Presence of Multivalent Ions. *J. Am. Chem. Soc.* **2020**, *142*, 14843−14847.
(14) Hughes, M. D. G.; Cussons, S.; Hanson, B. S.; Cook, K. R.; Feller, T.; Mahmoudi, N.; Baker, D. L.; Ariëns, R.; Head, D. A.; Brockwell, D. J.; Dougan, L. Building block aspect ratio controls assembly, architecture, and mechanics of synthetic and natural protein networks. *Nat. Commun.* **2023**, *14*, No. 5593.
(15) Hamley, I. W. Liquid crystal phase formation by biopolymers. *Soft Matter* **2010**, *6*, 1863−1871.
(16) Müllner, M.; Muller, A. H. E. Cylindrical polymer brushes - Anisotropic building blocks, unimolecular templates and particulate nanocarriers. *Polymer* **2016**, *98*, 389−401.
(17) Li, Z. L.; Tang, M.; Liang, S.; Zhang, M. Y.; Biesold, G. M.; He, Y. J.; Hao, S. M.; Choi, W.; Liu, Y. J.; Peng, J.; Lin, Z. Bottlebrush polymers: From controlled synthesis, self-assembly, properties to applications. *Prog. Polym. Sci.* **2021**, *116*, No. 101387.
(18) Zhao, B. Shape-Changing Bottlebrush Polymers. *J. Phys. Chem. B* **2021**, *125*, 6373−6389.
(19) Verduzco, R.; Li, X. Y.; Pesek, S. L.; Stein, G. E. Structure, function, self-assembly, and applications of bottlebrush copolymers. *Chem. Soc. Rev.* **2015**, *44*, No. 7916.
(20) Abbasi, M.; Faust, L.; Wilhelm, M. Comb and Bottlebrush Polymers with Superior Rheological and Mechanical Properties. *Adv. Mater.* **2019**, *31*, No. 1806484.
(21) Sheiko, S. S.; Sumerlin, B. S.; Matyjaszewski, K. Cylindrical molecular brushes: Synthesis, characterization, and properties. *Prog. Polym. Sci.* **2008**, *33*, 759−785.
(22) Pan, T.; Dutta, S.; Kamble, Y.; Patel, B. B.; Wade, M. A.; Rogers, S. A.; Diao, Y.; Guironnet, D.; Sing, C. E. Materials Design of Highly Branched Bottlebrush Polymers at the Intersection of Modeling, Synthesis, Processing, and Characterization. *Chem. Mater.* **2022**, *34*, 1990−2024.
(23) Xie, G.; Martinez, M. R.; Olszewski, M.; Sheiko, S. S.; Matyjaszewski, K. Molecular Bottlebrushes as Novel Materials. *Biomacromolecules* **2019**, *20*, 27−54.
(24) Nakagawa, Y.; Oki, Y.; Da, X.; Chandel, A. K. S.; Ohta, S.; Ito, T. Injectable bottlebrush triblock copolymer hydrogel crosslinked with ferric ions. *Polymer* **2022**, *240*, No. 124519.
(25) Keith, A. N.; Vatankhah-Varnosfaderani, M.; Clair, C.; Fahimipour, F.; Dashtimoghadam, E.; Lallam, A.; Sztucki, M.; Ivanov, D. A.; Liang, H. Y.; Dobrynin, A. V.; Sheiko, S. S. Bottlebrush Bridge between Soft Gels and Firm Tissues. *ACS Cent. Sci.* **2020**, *6*, 413−419.
(26) Yamauchi, Y.; Horimoto, N. N.; Yamada, K.; Matsushita, Y.; Takeuchi, M.; Ishida, Y. Two-Step Divergent Synthesis of Monodisperse and Ultra-Long Bottlebrush Polymers from an Easily Purifiable ROMP Monomer. *Angew. Chem., Int. Ed.* **2021**, *60*, 1528−1534.
(27) Blosch, S. E.; Scannelli, S. J.; Alaboalirat, M.; Matson, J. B. Complex Polymer Architectures Using Ring-Opening Metathesis Polymerization: Synthesis, Applications, and Practical Considerations. *Macromolecules* **2022**, *55*, 4200−4227.
(28) Clarke, B. R.; Witt, C. L.; Ilton, M.; Crosby, A. J.; Watkins, J. J.; Tew, G. N. Bottlebrush Networks: A Primer for Advanced Architectures. *Angew. Chem., Int. Ed.* **2024**, *63*, No. e202318220.
(29) Vatankhah-Varnosfaderani, M.; Keith, A. N.; Cong, Y.; Liang, H.; Rosenthal, M.; Sztucki, M.; Clair, C.; Magonov, S.; Ivanov, D. A.; Dobrynin, A. V.; Sheiko, S. S. Chameleon-like elastomers with molecularly encoded strain-adaptive stiffening and coloration. *Science* **2018**, *359*, 1509−1513.
(30) Sheiko, S. S.; Dobrynin, A. V. Architectural Code for Rubber Elasticity: From Supersoft to Superfirm Materials. *Macromolecules* **2019**, *52*, 7531−7546.
(31) Altay, E.; Nykypanchuk, D.; Rzayev, J. Mesoporous Polymer Frameworks from End-Reactive Bottlebrush Copolymers. *ACS Nano* **2017**, *11*, 8207−8214.
(32) Huang, K.; Rzayev, J. Well-Defined Organic Nanotubes from Multicomponent Bottlebrush Copolymers. *J. Am. Chem. Soc.* **2009**, *131*, 6880−6885.
(33) Bolton, J.; Bailey, T. S.; Rzayev, J. Large Pore Size Nanoporous Materials from the Self-Assembly of Asymmetric Bottlebrush Block Copolymers. *Nano Lett.* **2011**, *11*, 998−1001.
(34) Pang, X.; He, Y.; Jung, J.; Lin, Z. 1D nanocrystals with precisely controlled dimensions, compositions, and architectures. *Science* **2016**, *353*, 1268−1272.
(35) Müllner, M.; Dodds, S. J.; Nguyen, T.-H.; Senyschyn, D.; Porter, C. J. H.; Boyd, B. J.; Caruso, F. Size and Rigidity of Cylindrical Polymer Brushes Dictate Long Circulating Properties In Vivo. *ACS Nano* **2015**, *9*, 1294−1304.
(36) Xu, L.; Zhang, Q.; Lu, L.; Shi, Y.; Liu, L.; Shen, J.; Chen, Y. Unimolecular Nano-contrast Agent with Ultrahigh Relaxivity and Very Long Retention for Magnetic Resonance Lymphography. *Nano Lett.* **2022**, *22*, 4090−4096.
(37) Piunova, V. A.; Miyake, G. M.; Daeffler, C. S.; Weitekamp, R. A.; Grubbs, R. H. Highly Ordered Dielectric Mirrors via the Self-Assembly of Dendronized Block Copolymers. *J. Am. Chem. Soc.* **2013**, *135*, 15609−15616.
(38) Song, D.-P.; Li, C.; Li, W.; Watkins, J. J. Block Copolymer Nanocomposites with High Refractive Index Contrast for One-Step Photonics. *ACS Nano* **2016**, *10*, 1216−1223.
(39) Song, D.-P.; Zhao, T. H.; Guidetti, G.; Vignolini, S.; Parker, R. M. Hierarchical Photonic Pigments via the Confined Self-Assembly of Bottlebrush Block Copolymers. *ACS Nano* **2019**, *13*, 1764−1771.
(40) Vashahi, F.; Martinez, M. R.; Dashtimoghadam, E.; Fahimipour, F.; Keith, A. N.; Bersenev, E. A.; Ivanov, D. A.; Zhulina, E. B.; Popryadukhin, P.; Matyjaszewski, K.; et al. Injectable bottlebrush hydrogels with tissue-mimetic mechanical properties. *Sci. Adv.* **2022**, *8*, No. eabm2469.
(41) Ohnsorg, M. L.; Mash, K. M.; Khang, A.; Rao, V. V.; Kirkpatrick, B. E.; Bera, K.; Anseth, K. S. Nonlinear Elastic Bottlebrush Polymer Hydrogels Modulate Actomyosin Mediated Protrusion Formation in Mesenchymal Stromal Cells. *Adv. Mater.* **2024**, *36*, No. 2403198.
(42) Harrington, M. J.; Fratzl, P. Natural load-bearing protein materials. *Prog. Mater. Sci.* **2021**, *120*, No. 100767.
(43) Fratzl, P.; Weinkamer, R. Nature's hierarchical materials. *Prog. Mater. Sci.* **2007**, *52*, 1263−1334.
(44) Paturej, J.; Sheiko, S. S.; Panyukov, S.; Rubinstein, M. Molecular structure of bottlebrush polymers in melts. *Sci. Adv.* **2016**, *2*, No. e1601478.
(45) Sarapas, J. M.; Martin, T. B.; Chremos, A.; Douglas, J. F.; Beers, K. L. Bottlebrush polymers in the melt and polyelectrolytes in solution share common structural features. *Proc. Natl. Acad. Sci. U.S.A.* **2020**, *117*, 5168−5175.
(46) Wintermantel, M.; Fischer, K.; Gerle, M.; Ries, R.; Schmidt, M.; Kajiwara, K.; Urakawa, H.; Wataoka, I. Lyotropic Phases Formed by Molecular Bottlebrushes. *Angew. Chem. Int. Ed.* **1995**, *34*, 1472−1474.
(47) Rathgeber, S.; Pakula, T.; Wilk, A.; Matyjaszewski, K.; Lee, H. I.; Beers, K. L. Bottle-brush macromolecules in solution: Comparison between results obtained from scattering experiments and computer simulations. *Polymer* **2006**, *47*, 7318−7327.
(48) Sunday, D. F.; Burns, A. B.; Martin, T. B.; Chang, A. B.; Grubbs, R. H. Relationship between Graft Density and the Dilute Solution Structure of Bottlebrush Polymers: An Inter-chemistry Comparison and Scaling Analysis. *Macromolecules* **2023**, *56*, 7419−7431.
(49) Wintermantel, M.; Fischer, K.; Gerle, M.; Ries, R.; Schmidt, M.; Kajiwara, K.; Urakawa, H.; Wataoka, I. Lyotropic Phases Formed by "Molecular Bottlebrushes. *Angew. Chem., Int. Ed.* **1995**, *34*, 1472−1474.
(50) Sun, H.; Qiao, B.; Choi, W.; Hampu, N.; McCallum, N. C.; Thompson, M. P.; Oktawiec, J.; Weigand, S.; Ebrahim, O. M.; de la

Cruz, M. O.; Gianneschi, N. C. Origin of Proteolytic Stability of Peptide-Brush Polymers as Globular Proteomimetics. *ACS Cent. Sci.* **2021**, *7*, 2063−2072.
(51) Walsh, D. J.; Guironnet, D. Macromolecules with programmable shape, size, and chemistry. *Proc. Natl. Acad. Sci. U.S.A.* **2019**, *116*, 1538−1542.
(52) Jha, S.; Dutta, S.; Bowden, N. B. Synthesis of ultralarge molecular weight bottlebrush polymers using Grubbs' catalysts. *Macromolecules* **2004**, *37*, 4365−4374.
(53) Leo, C. M.; Jang, J.; Corey, E. J.; Neary, W. J.; Bowman, J. I.; Kennemur, J. G. Comparison of Polypentenamer and Polynorbornene Bottlebrushes in Dilute Solution. *ACS Polym. Au* **2024**, *4*, 235−246.
(54) Sumerlin, B. S.; Neugebauer, D.; Matyjaszewski, K. Initiation Efficiency in the Synthesis of Molecular Brushes by Grafting from via Atom Transfer Radical Polymerization. *Macromolecules* **2005**, *38*, 702−708.
(55) Min, K.; Yu, S.; Lee, H.-i.; Mueller, L.; Sheiko, S. S.; Matyjaszewski, K. High Yield Synthesis of Molecular Brushes via ATRP in Miniemulsion. *Macromolecules* **2007**, *40*, 6557−6563.
(56) Dutertre, F.; Bang, K.-T.; Loppinet, B.; Choi, I.; Choi, T.-L.; Fytas, G. Structure and Dynamics of Dendronized Polymer Solutions: Gaussian Coil or Macromolecular Rod? *Macromolecules* **2016**, *49*, 2731−2740.
(57) Radzinski, S. C.; Foster, J. C.; Chapleski, R. C.; Troya, D.; Matson, J. B. Bottlebrush Polymer Synthesis by Ring-Opening Metathesis Polymerization: The Significance of the Anchor Group. *J. Am. Chem. Soc.* **2016**, *138*, 6998−7004.
(58) Scannelli, S. J.; Alaboalirat, M.; Troya, D.; Matson, J. B. Influence of the Norbornene Anchor Group in Ru-Mediated Ring-Opening Metathesis Polymerization: Synthesis of Bottlebrush Polymers. *Macromolecules* **2023**, *56*, 3838−3847.
(59) Blosch, S. E.; Alaboalirat, M.; Eades, C. B.; Scannelli, S. J.; Matson, J. B. Solvent Effects in Grafting-through Ring-Opening Metathesis Polymerization. *Macromolecules* **2022**, *55*, 3522−3532.
(60) Holerca, M. N.; Peterca, M.; Partridge, B. E.; Xiao, Q.; Lligadas, G.; Monteiro, M. J.; Percec, V. Monodisperse Macromolecules by Self-Interrupted Living Polymerization. *J. Am. Chem. Soc.* **2020**, *142*, 15265−15270.
(61) Gu, Y.; Zhao, J.; Johnson, J. A. Polymer Networks: From Plastics and Gels to Porous Frameworks. *Angew. Chem., Int. Ed.* **2020**, *59*, 5022−5049.
(62) Gao, H.; Matyjaszewski, K. Synthesis of functional polymers with controlled architecture by CRP of monomers in the presence of cross-linkers: From stars to gels. *Prog. Polym. Sci.* **2009**, *34*, 317−350.
(63) Ribelli, T. G.; Lorandi, F.; Fantin, M.; Matyjaszewski, K. Atom Transfer Radical Polymerization: Billion Times More Active Catalysts and New Initiation Systems. *Macromol. Rapid Commun.* **2019**, *40*, No. 1800616.
(64) Szczepaniak, G.; Jeong, J.; Kapil, K.; Dadashi-Silab, S.; Yerneni, S. S.; Ratajczyk, P.; Lathwal, S.; Schild, D. J.; Das, S. R.; Matyjaszewski, K. Open-air green-light-driven ATRP enabled by dual photoredox/copper catalysis. *Chem. Sci.* **2022**, *13*, 11540−11550.
(65) Hu, X.; Szczepaniak, G.; Lewandowska-Andralojc, A.; Jeong, J.; Li, B.; Murata, H.; Yin, R.; Jazani, A. M.; Das, S. R.; Matyjaszewski, K. Red-Light-Driven Atom Transfer Radical Polymerization for High-Throughput Polymer Synthesis in Open Air. *J. Am. Chem. Soc.* **2023**, *145*, 24315−24327.
(66) Hu, X.; Yin, R.; Jeong, J.; Matyjaszewski, K. Robust Miniemulsion PhotoATRP Driven by Red and Near-Infrared Light. *J. Am. Chem. Soc.* **2024**, *146*, 13417−13426.
(67) Jeong, J.; Hu, X.; Yin, R.; Fantin, M.; Das, S. R.; Matyjaszewski, K. Nucleic Acid-Binding Dyes as Versatile Photocatalysts for Atom-Transfer Radical Polymerization. *J. Am. Chem. Soc.* **2024**, *146*, 13598−13606.
(68) Martinez, M. R.; Sobieski, J.; Lorandi, F.; Fantin, M.; Dadashi-Silab, S.; Xie, G.; Olszewski, M.; Pan, X.; Ribelli, T. G.; Matyjaszewski, K. Understanding the Relationship between Catalytic Activity and Termination in photoATRP: Synthesis of Linear and Bottlebrush Polyacrylates. *Macromolecules* **2020**, *53*, 59−67.
(69) Neugebauer, D.; Sumerlin, B. S.; Matyjaszewski, K.; Goodhart, B.; Sheiko, S. S. How dense are cylindrical brushes grafted from a multifunctional macroinitiator? *Polymer* **2004**, *45*, 8173−8179.
(70) Bak, J. M.; Jha, G.; Ahn, E.; Jung, S.-H.; Jeong, H. M.; Kim, B.-S.; Lee, H.-i. Molecular brushes with extreme grafted side chain densities. *Polymer* **2012**, *53*, 3462−3468.
(71) Burdyńska, J.; Daniel, W.; Li, Y.; Robertson, B.; Sheiko, S. S.; Matyjaszewski, K. Molecular Bottlebrushes with Bimodal Length Distribution of Side Chains. *Macromolecules* **2015**, *48*, 4813−4822.
(72) Walsh, D. J.; Wade, M. A.; Rogers, S. A.; Guironnet, D. Challenges of Size-Exclusion Chromatography for the Analysis of Bottlebrush Polymers. *Macromolecules* **2020**, *53*, 8610−8620.
(73) Sheiko, S. S.; Sun, F. C.; Randall, A.; Shirvanyants, D.; Rubinstein, M.; Lee, H.; Matyjaszewski, K. Adsorption-induced scission of carbon-carbon bonds. *Nature* **2006**, *440*, 191−194.
(74) Jung, J.-M.; Mezzenga, R. Liquid Crystalline Phase Behavior of Protein Fibers in Water: Experiments versus Theory. *Langmuir* **2010**, *26*, 504−514.
(75) Gillespie, D.; Rouzeau, S.; Lu, W.; Soleymannezhad, A. Characterization of Polymers by LenS3 Multiangle Light Scattering. In *Molecular Characterization of Polymers*; Malik, M. I.; Mays, J.; Shah, M. R., Eds.; Elsevier, 2021; Chapter 14, pp 533−559.
(76) Detappe, A.; Nguyen, H. V. T.; Jiang, Y.; Agius, M. P.; Wang, W.; Mathieu, C.; Su, N. K.; Kristufek, S. L.; Lundberg, D. J.; Bhagchandani, S.; et al. Molecular bottlebrush prodrugs as mono- and triplex combination therapies for multiple myeloma. *Nat. Nanotechnol.* **2023**, *18*, 184−192.

https://doi.org/10.1021/jacs.4c13759
J. Am. Chem. Soc. 2025, 147, 889−897